IOPscience iopscience.iop.org

Home Search Collections Journals About Contact us My IOPscience

Ultra-low resistive GaSb/InAs tunnel junctions

This content has been downloaded from IOPscience. Please scroll down to see the full text.

2011 Semicond. Sci. Technol. 26 075021

(http://iopscience.iop.org/0268-1242/26/7/075021)

View the table of contents for this issue, or go to the journal homepage for more

Download details:

IP Address: 128.97.245.226
This content was downloaded on 26/12/2014 at 17:32

Please note that terms and conditions apply.

IOP PUBLISHING SEMICONDUCTOR SCIENCE AND TECHNOLOGY
Semicond. Sci. Technol. **26** (2011) 075021 (4pp) doi:10.1088/0268-1242/26/7/075021

Ultra-low resistive GaSb/InAs tunnel junctions

Kristijonas Vizbaras, Marcel Törpe, Shamsul Arafin and Markus-Christian Amann

Walter Schottky Institut, Technische Universität München, Am Coulombwall 3, Garching, 85478, Germany

E-mail: kristijonas.vizbaras@wsi.tum.de

Received 7 February 2011, in final form 28 March 2011
Published 15 April 2011
Online at stacks.iop.org/SST/26/075021

Abstract
The GaSb and InAs(Sb) material combination results in a type-III (broken gap) band alignment and is of particular interest for use as an ohmic, low-resistive intra-cavity contact in complex optoelectronic devices, such as buried-tunnel-junction vertical-cavity surface-emitting lasers. In this work, we report electrical characteristics of MBE-grown p^+-GaSb/n^+-InAs tunnel junctions. The investigated structures exhibit ultra-low resistive behavior, yielding specific resistivity values below $2.8 \times 10^{-7} \Omega$ cm^2. This value is nearly ten times better than previously reported best values.

(Some figures in this article are in colour only in the electronic version)

1. Introduction

Development of GaSb-based optoelectronic devices has received a lot of interest recently. This is mainly due to emerging applications such as trace gas sensing by means of tunable diode laser absorption spectroscopy (TDLAS) [1–3], which requires devices that are able to emit or detect light in the near- and mid-infrared spectral region. An emitter in a TDLAS sensor has to fulfill several requirements. For instance, it has to be (electro-thermally) tunable, operate in a single mode and exhibit continuous-wave (CW) operation. This is met by two diode laser sources—distributed-feedback (DFB) laser and vertical-cavity surface-emitting laser (VCSEL)—out of which the VCSEL is preferable due to its wide tuning range, good beam quality, compactness and low power consumption. In order to operate in CW and emit in a single transversal mode, a VCSEL requires a small current aperture. In GaSb-based VCSELs, this is achieved by implementing a buried-tunnel junction (BTJ) as an intra-cavity electrical contact [4–6]. A BTJ is a key component in such devices, because it allows the substitution of p-doped by an n-doped material, resulting in lower heating and losses. Moreover, it serves as a current aperture, confining the current to the active region, leading to small laser threshold currents and CW operation. It is very important that a BTJ is low resistive, in order to avoid excessive heating of the device at high current densities. Typically, in GaSb-based devices a p^+-GaSb/n^+-InAsSb heterojunction is used for a BTJ [6]. Such a material combination results in a type-III (broken gap) band alignment and inherently favors tunneling, which should enhance the performance of such a junction and lead to low resistivities. Moreover, low effective masses of GaSb, InAs and InAsSb should enhance the tunneling compared to InP-based tunnel junctions. However, up to now, this has not been confirmed experimentally—record values for GaSb-based BTJs ($2.4 \times 10^{-6} \Omega$ cm^2) [7] that have been reported were only similar to the best ones for InP-based structures ($3 \times 10^{-6} \Omega$ cm^2) [8].

In this work, we present the performance of MBE-grown p^+-GaSb/n^+-InAs tunnel junctions with ultra-low resistivities below $2.8 \times 10^{-7} \Omega$ cm^2. This is by an order of magnitude better than previously reported values for InP- and GaSb-based material systems.

2. Device growth and fabrication

A single tunnel junction and five vertically stacked tunnel-junction-device structures were grown by a solid-source Varian Mod Gen-II MBE reactor with valved cracker cells for Sb_2 and As_2. Growth temperature was evaluated by means of optical pyrometry and calibrated to GaSb oxide desorption temperature (about 550 °C). The schematic view of a test structure is shown in figure 1. The growth of epitaxial

 © 2011 IOP Publishing Ltd Printed in the UK & the USA

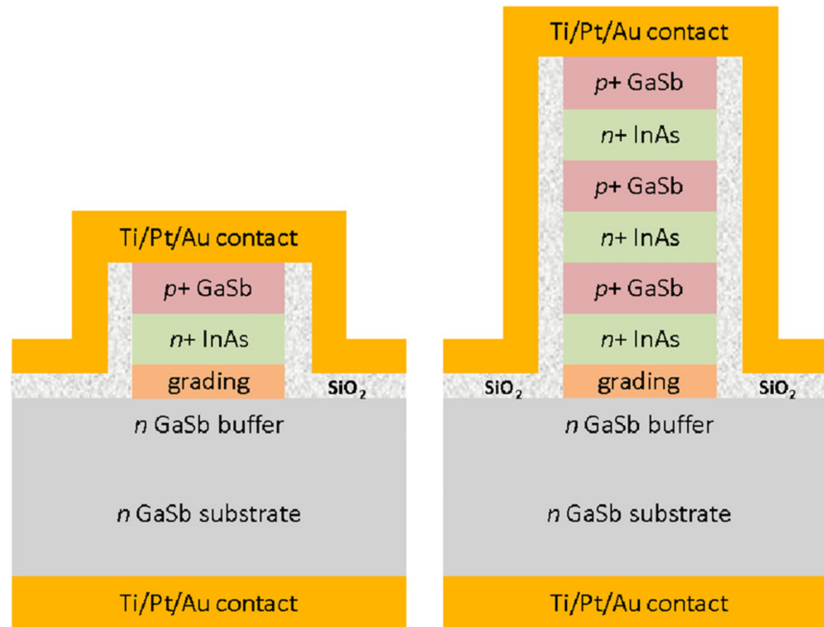

Figure 1. Schematic cross-sectional view of a single-tunnel-junction device (left) and a five-tunnel-junction device (right) used for tunnel contact measurements. In both structures corresponding layer structures are the same: 8 nm thick grading, 20 nm thick p^+-GaSb and 20 nm thick n^+-InAs.

structures was performed on Te-doped n-GaSb substrates. First, a 300 nm thick n-GaSb ($5 \times 10^{17}\text{cm}^{-3}$) buffer layer was grown at 500 °C in order to reduce the influence of the defects remaining from the thermal oxide desorption step. Then, the substrate temperature was ramped down to 400 °C under Sb_2 stabilization for the growth of the tunnel-junction layers. The growth was proceeded by an 8 nm thick digitally alloyed Te-doped ($1 \times 10^{19}\text{cm}^{-3}$) InAs/GaSb grading layer, in order to reduce the resistivity at the heterointerface. Finally, tunnel-junction layers were grown, starting with a 20 nm thick Si-doped n^+-InAs ($1 \times 10^{19}\text{cm}^{-3}$) layer and finishing with a 20 nm Si-doped p^+-GaSb ($1 \times 10^{19}\text{cm}^{-3}$) layer. Si simultaneously acts as a p-dopant in GaSb and as an n-dopant in InAs(Sb). In the case of vertically stacked five tunnel junctions, the layer thicknesses were the same as for a single-tunnel-junction device (20 nm InAs and 20 nm GaSb).

After the growth, device structures were processed. Processing started with a definition of circular mesas by means of UV-lithography, followed by a subsequent dry-etching procedure. Here, it is important to etch through the GaSb/InAs layers into the buffer layer, in order to have a defined current confinement. After etching, mesa sidewalls were passivated with 200 nm thick sputtered SiO_2, and contact windows were opened by a subsequent lift-off in acetone. The contact window size in all cases coincided with the mesa diameter. Samples were then dipped in concentrated HCl to remove the oxides that formed during the previous processing steps and a thin controlled layer of oxide was deposited by systematically diluting the HCl solution with de-ionized water. Then, the samples were immersed in an aqueous $(NH_4)_2S$ solution in order to exchange the oxygen with sulfur and passivate the dangling bonds at the surface. A more detailed description of the procedure can be found in [9]. The wet-chemical passivation step was followed by an immediate loading of the samples into a metal-deposition chamber. For the top contact Ti/Pt/Au was used, as is known to form an ohmic, low-resistive contact on p-GaSb [10]. The size of the top contact pad was 400 × 400 μm for all diameters. Also on the backside Ti/Pt/Au was evaporated.

3. Device results and discussion

Current-voltage (I–V) characteristics of the test structures were measured. Here, one has to keep in mind that the total measured resistance R_{EXP} is comprised of several components—backside metal–semiconductor contact resistance R_B, resistance of the tunnel-junction layers R_{TJ}, substrate resistance R_S and top metal–semiconductor contact resistance R_{MS}. The measured resistance is then expressed in the following way:

$$R_{\text{EXP}} = R_B + R_S + R_{\text{TJ}} + R_{\text{MS}}. \quad (1)$$

Since the current can spread over a 500 μm thick n-GaSb substrate, the resistance caused by the backside contact can be neglected ($R_B < 1 \times 10^{-4}\Omega$). Additionally, one can separate the contribution of the substrate resistance and the sum of the tunnel-junction layers and top metal–semiconductor contact from the measured value, because of a different dependence on the mesa diameter: $R_S \sim 1/d$ and $(R_{\text{TJ}} + R_{\text{MS}}) \sim 1/d^2$. Here, d is the mesa diameter. The final extraction of the individual components that constitute the experimentally measured resistance R_{EXP} is rather complicated, because the spreading of the current in the substrate is also dependent on the mesa width. A method dealing with such a situation is described in detail in [11]. There, a radius-dependant potential $U(r)$, caused by the current distribution $j(r)$, is evaluated. The potential at the contact pad U_0 is considered constant and

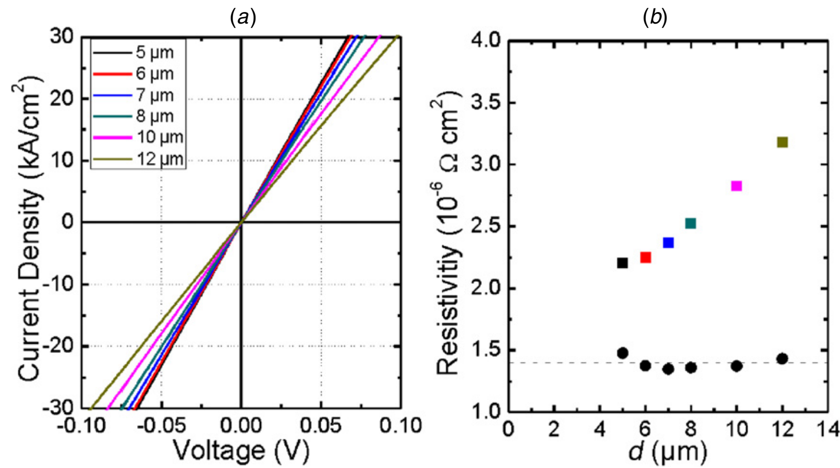

Figure 2. (*a*) Measured current density–voltage (*j*–*U*) characteristics for different mesa diameters of a five-tunnel-junction sample. Spreading of *j*–*U* characteristics due to substrate current crowding is clearly visible; (*b*) Measured total resistivity of a five-tunnel-junction sample for different diameters (colored squares) and extracted resistivity of the tunnel-junction layers and top metal–semiconductor contact (full circles). The colors correspond to *j*–*U* characteristics of mesas with different diameters in figure 2(*a*).

the radius-dependent potential at the semiconductor surface is observed. Both potentials are linked together by the contact resistance ρ_C between metal and semiconductor interface:

$$j(r) = \frac{U_0 - U(r)}{\rho_C}. \quad (2)$$

In our case we cannot distinguish between the top metal–semiconductor contact resistance and the resistance of tunnel-junction layers, but we can subtract the substrate contribution as in [11] and estimate the upper limit of the resistivity, caused by tunnel-junction layers. Equation (2) is solved in [11] for a circular point-contact geometry. Simple extraction of the contact resistance $\rho_C = AR_{\mathrm{EXP}}$, where A is area in cm^2 and R_{EXP} is the measured resistance, becomes erroneous for

$$\frac{\rho_C}{\pi r^2} \leqslant \frac{\rho_S}{4r}. \quad (3)$$

Here, ρ_S is the substrate resistivity, which is used as a variable to get the best fit for contact resistivity. Therefore, a more accurate technique, based on [11] has been applied. The total resistivity $\rho_{\mathrm{tot}} = U/j$, with U being the applied voltage and j the current density, consists of contributions from the contact and substrate. The contact resistivity, in our case, can be accurately extracted using an approximation from the exact method in [11] as

$$\rho_C = A\left(R_{\mathrm{EXP}} - \frac{\rho_S}{2d}\right). \quad (4)$$

Equation (4) approximates the total resistance as the sum of substrate and contract resistance, which is a reasonable approximation as long as the measured resistance R_{EXP} is not too close to the substrate resistance $\frac{\rho_S}{2d}$. For a single tunnel junction, the measured mesa resistance was found to be in very close proximity of the substrate-induced limit ($R_S(d = 6\ \mu\mathrm{m}) = \frac{\rho_S}{4r} = \frac{\rho_S}{2d} = \frac{6\times10^{-3}\Omega\ \mathrm{cm}}{2.6\times10^{-4}\ \mathrm{cm}} = 5\Omega$ for a 6 μm wide mesa). Accordingly, the contact resistivity is very small and not accurately measurable using only one tunnel junction. In order to increase the accuracy, five tunnel junctions were grown in series, as shown in figure 1. According to our 8 band $k \cdot p$ simulations, performed with nextnano++,[1] the quantum confinement effects are not strong for our five-tunnel-junction structure with given layer thicknesses and linearity of scaling holds. The latter strategy was chosen in order to evaluate the resistivity of tunnel-junction layers subtracting the contributions of the top metal–semiconductor contact. Different diameters were investigated in order to rule out any errors in obtained results, related to geometrical fluctuations due to process uncertainties. Figure 2(*a*) shows the measured *j*–*U* characteristics for different diameters of a five-tunnel-junction structure and figure 2(*b*) shows the measured $\left(\rho_{\mathrm{total}} = \frac{U}{j}\right)$ and extracted contact resistivities (ρ_C) as a function of the mesa diameter. Measured devices exhibit purely ohmic behavior in the current density range of –30 to +30 kA cm^{-2}.

As can be seen from figures 2(*a*) and (*b*), the measured resistance is still strongly influenced by the current crowding in the substrate, even though we are measuring five tunnel junctions in series. The extracted value for the sum of five tunnel junctions and top metal–semiconductor contact yields a value of $1.4 \times 10^{-6}\Omega$ cm^2, implying that the resistivity of a single n$^+$-InAs/p$^+$-GaSb tunnel junction is lower than $2.8 \times 10^{-7}\Omega$ cm^2. This result is nearly ten times better than the previously reported record value with InAsSb/GaSb tunnel junction ($2.4 \times 10^{-6}\Omega$ cm^2) [7] (see figure 3) and InP-based ($3 \times 10^{-6}\Omega$ cm^2) one [8]. This striking improvement, when compared to InP-based tunnel junctions, can be attributed to a broken gap band alignment between InAs(Sb) and GaSb, which inherently favors tunneling. Moreover, lower effective masses of the carriers in InAs and GaSb lead to an enhancement of the tunneling probability [12]. Regarding the difference in performance between the previously reported [7] and our work, we believe that the main improvement lies in the optimization of the epitaxial growth.

For our tunnel junction growth we took special care when forming the interface between InAs and GaSb. First of all,

[1] For obtaining Nextnano executables and related publications [online] http://www.wsi.tum.de/nextnano.

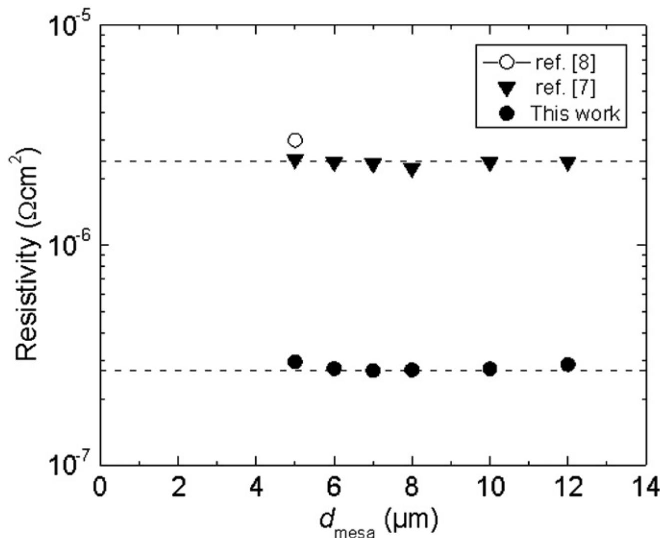

Figure 3. Resistivity as a function of the mesa diameter for a single GaSb-tunnel junction (full triangles) from [7], InP-based one (open circle) from [8] and the result achieved in this work (full circles). Here, a single-tunnel-junction resistivity also has a contribution from the top metal–semiconductor contact.

we removed the excess arsenic due to group-V overpressure when growing the InAs layer. The removal was done by introducing a growth interruption after the layer, during which As_2 stabilization was turned off and excess arsenic desorbed [13] by leaving the surface slightly In-rich. Second, we soaked the InAs surface with Sb_2 for several seconds, in order to create InSb-like and GaSb-like interfaces [14, 15], which favor tunneling transport. Additionally, InAs has been used instead of InAsSb, in order to avoid unwanted effects related to Sb surface segregation [16], which could have a negative effect on the transport properties of the layer and, especially, the heterointerface.

4. Summary and conclusions

To summarize, in this work we report ultra-low resistive n^+-InAs/p^+-GaSb tunnel junctions with resistivities below $2.8 \times 10^{-7}\Omega$ cm^2, which is by an order of magnitude better than previously reported values. Such a performance can be attributed to an optimized MBE growth technique, which allowed the reduction of excess arsenic on the InAs surface and the creation of InSb-like and GaSb-like bonds at the heterointerface.

Acknowledgment

This work has been supported by the European Union via NEMIS (contract no FP6-2005-IST-5-031845).

References

[1] Vicet P A, Yarekha D A, Perona A, Rouillard Y, Gaillard S and Baranov A N 2002 Trace gas detection with antimonide-based quantum-well diode lasers *Spectrochim. Acta* A **58** 2405

[2] Werle P 1998 A review of recent advances in semiconductor laser based gas monitors *Spectrochim. Acta* A **54** 197–236

[3] Werle P, Slemr F, Maurer K, Kormann R, Mücke R and Jänker B 2002 Near- and mid-infrared laser-optical sensors for gas analysis *Opt. Lasers Eng.* **37** 101–14

[4] Bachmann A, Lim T, Kashani-Shirazi K, Dier O, Lauer C and Amann M-C 2008 Continuous-wave operation of electrically pumped GaSb-based vertical cavity surface emitting laser at 2.3 μm *Electron. Lett.* **44** 202–3

[5] Arafin S, Bachmann A, Kashani-Shirazi K and Amann M-C 2009 Electrically pumped continuous-wave vertical-cavity surface-emitting lasers at $\sim$ 2.6 μm *Appl. Phys. Lett.* **95** 131120

[6] Dier O, Sterkel M, Grau M, Lin C, Lauer C and Amann M-C 2004 Tunnel junctions for ohmic intra-device contacts on GaSb-substrates *Appl. Phys. Lett.* **85** 2388

[7] Dier O, Lauer C and Amann M-C 2006 n-InAsSb/p-GaSb tunnel junctions with extremely low resistivity *Electron. Lett.* **42** 419–20

[8] Ortsiefer M, Shau R, Böhm G, Köhler F, Abstreiter G and Amann M-C 2000 Low resistance InGa(Al)As tunnel junctions for long wavelength vertical-cavity surface-emitting lasers *Japan. J. Appl. Phys.* **39** 1727

[9] Arafin S, Bachmann A, Kashani-Shirazi K, Priyabadini S and Amann M-C 2009 Low-resistive sulphur-treated ohmic contacts to n-type InAsSb *IET Opt.* **3** 259

[10] Vogt A, Simon A, Weber J, Hartnagel H L, Schikor J, Buschmann V and Fuess H 1999 Non-annealed ohmic contacts to p-GaSb grown by molecular beam epitaxy *Mater. Sci. Eng.* B **66** 199

[11] Franz G and Amann M-C 1993 Extremely low contact resistivity of Ti/Pt/Au contacts on p+-InGaAs as determined by a new evaluation method *J. Electrochem. Soc.* **140** 847

[12] Kane E O 1961 Theory of tunneling *J. Appl. Phys.* **32** 83

[13] Liang B W and Tu C W 1993 A study of group-V element desorption from InAs, InP, GaAs and GaP by reflection high-energy electron diffraction *J. Cryst. Growth* **128** 538

[14] Khoshakhlagh A, Plis E, Myers S, Sharma Y, Dawson L and Krishna S 2009 Optimization of InAs/GaSb type-II superlattice interfaces for long-wave (8 μm) infrared detection *J. Cryst. Growth* **311** 1901

[15] Khoshakhlagh A, Myers S, Kim H, Plis E, Gautam L N, Lee S J, Noh S K, Dawson L R and Krishna S 2010 Long wave InAs/GaSb superlattice detectors based on nBn and PIN designs *IEEE J. Quantum Electron.* **46** 959

[16] Miyoshi H, Suzuki R, Amano H and Horikoshi Y 2002 Sb surface segregation effect on the phase separation of MBE grown InAsSb *J. Cryst. Growth* **237** 1519